

The Double Spin Asymmetry of Nitrogen in Elastic and Quasielastic Kinematics from a Solid Ammonia Dynamically Polarized Target

M. Friedman^{a,1,*}, J. Campbell^{b,c,d}, D. Day^e, D.W. Higinbotham^c, A. Sarty^d, G. Ron^a

^a*Racah Institute of Physics, Hebrew University, Jerusalem, Israel 91904*

^b*Dalhousie University, Halifax, Nova Scotia B3H 4R2, Canada*

^c*Thomas Jefferson National Accelerator Facility, Newport News, VA 23606, USA*

^d*Saint Marys University, Halifax, Nova Scotia B3H 3C3, Canada*

^e*University of Virginia, Charlottesville, VA, 22904, USA*

Abstract

Solid ammonia (NH_3) is commonly used as a dynamically polarized proton target for electron and muon scattering cross-section asymmetry measurements. As spin 1^+ particles, the ^{14}N nuclei in the target are also polarized and contribute a non-trivial asymmetry background that should be addressed. We describe here a method to extract the nitrogen contribution to the asymmetry, and report the cross-section asymmetries of electron-nitrogen scattering at beam energies of $E = 1.7$ GeV and $E = 2.2$ GeV, and momentum transfer of $Q^2 = 0.023\text{--}0.080$ GeV^2 .

Keywords: DNP, Nitrogen Asymmetry, Proton Form Factor, DSA

1. Introduction

Scattering experiments of polarized lepton beams off polarized proton and other light targets has been used in the last few decades as a powerful tool for precision measurement of the nuclear electromagnetic form factors and spin structure functions (see, for example, Refs. [1–8]). Solid ammonia, $^{14}\text{NH}_3$, is

*Corresponding author

Email address: moshe.friedman@mail.huji.ac.il (M. Friedman)

¹Current address: National Superconducting Cyclotron Laboratory, Michigan State University, East Lansing, Michigan 48824, USA

commonly used as a polarized proton target by exploiting the Dynamic Nuclear Polarization (DNP) technique to achieve proton polarizations over 90% [9–12].

Previous works has shown that the spin 1^+ ^{14}N is also polarized in the process to approximately 10%, and hence contributes a nontrivial background to scattering asymmetry experiments [13–16]. Specifically, experiments that utilize the asymmetry of the scattering cross section as a probe of the nucleon structure must take into account the asymmetry contribution by the polarized nitrogen nuclei. However, direct experimental data of the background contribution to the measured asymmetry is not yet available.

JLab experiment E08-007, GEp, measured the proton elastic form factor ratio, $\mu G_E/G_M$, at low momentum transfer, using elastic scattering of a polarized electron beam from a polarized $^{14}\text{NH}_3$ target [17]. In this report we present an analysis approach used to disentangle the nitrogen contribution to the asymmetry from the proton asymmetry. In addition, we report for the first time experimental cross section asymmetries of ^{14}N elastic and quasi-elastic electron scattering.

2. Experimental Setup

The goal of the GEp experiment was to measure the proton elastic form factor ratio at a Q^2 range of 0.01-0.08 GeV^2 , using the double spin asymmetry (DSA) technique [18]. The experiment was performed in Hall A of the Continuous Electron Beam Accelerator Facility (CEBAF) at the Thomas Jefferson National Accelerator Facility [19, 20]. A schematic view of the experimental setup is shown in Fig. 1. The CEBAF polarized beam at energies of 1.7 and 2.2 GeV, passed through fast and slow rasters and use two chicane magnets to compensate for the effect of the target magnetic field. The electrons, scattered off the polarized NH_3 target (Sec. 2.1) and bent by the septum magnet, were detected by one of two High Resolution Spectrometers, HRSs. The beam current of ~ 10 nA used for this experiment was too low to allow beam position monitoring [17].

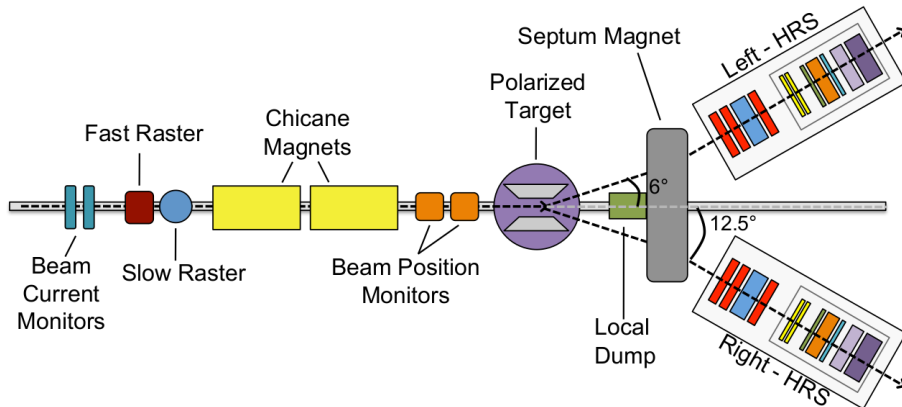


Figure 1: Schematic diagram of the GEp experimental setup. See text for description. Figure from Ref. [21].

The target was polarized by a 5 T magnetic field, 5.6° left of the beam axis. The transverse component of the field causes downwards deflection of the beam. To compensate for this effect, two chicane magnets were installed 5.92 m and 2.66 m upstream of the target. The two dipole magnets were tuned to direct the deflected beam towards the center of the target.

The data was taken at forward angles of $\sim 4^\circ - 7^\circ$. Due to technical limitations, the HRSs could not be placed at angles less than 12.5° . For this reason, the target was placed 88 cm upstream of the traditional Hall A center, and two septum magnets were installed in front of the spectrometer to direct the scattered electrons from the forward angles to the actual HRSs position.

The data was taken using the standard Hall A HRS spectrometers [20], and the analysis reported here is based on the left HRS data. The beam polarization level was measured before, between, and after production runs of GEp, using the Hall A Møller polarimeter [20, 22] (see Table 1).

2.1. Polarized NH_3 target

A highly polarized proton target was needed for the GEp experiment. For this, we used the UVa solid NH_3 target [10–12] that was successfully used for several experiments at JLab [6, 24]. The target operates at a temperature of

date	beam polarization
03/03/2012	-79.91 ± 0.20
03/30/2012	-80.43 ± 0.46
03/30/2012	+79.89 ± 0.58
04/10/2012	-88.52 ± 0.30
04/23/2012	+89.72 ± 0.29
05/04/2012	-83.47 ± 0.57
05/04/2012	-81.82 ± 0.59
05/04/2012	+80.40 ± 0.45
05/15/2012	+83.59 ± 0.31

Table 1: Beam polarization as measured by Møller polarimetry. Quoted uncertainties are statistical. Systematic uncertainties are estimated to be 1.7% for all measurements. For details see [23].

~1 K, with a 5 T magnetic field. The protons are polarized via the Dynamic Nuclear Polarization (DNP) technique [25, 26]. For a detailed description of the target see [27, 28] and references therein.

2.1.1. Dynamic Nuclear Polarization

Target polarization is defined as the difference between positive and negative aligned nuclear spins relative to the polarization axis, divided by the total number of nuclear spins:

$$P = \frac{N_{\uparrow} - N_{\downarrow}}{N_{\uparrow} + N_{\downarrow}}. \quad (1)$$

A traditional polarization technique is Thermal equilibrium (TE) polarization, also called brute force polarization, where the target is cooled to low temperatures in a high magnetic field. In that case, the population of two magnetic sub levels is determined by the Boltzmann distribution:

$$N_1 = N_2 \cdot \exp\left(-\frac{\Delta E}{k_B T}\right), \quad (2)$$

where ΔE is the energy difference between the levels, T is target temperature, k_B is the Boltzmann constant, and $N_{1,2}$ are the number of nuclear spins in each

sub level. For a spin-1/2 target, the polarization level obtained by TE is:

$$P = \tanh\left(\frac{g\mu B}{2k_B T}\right). \quad (3)$$

Here g is the particle g-factor, and μ is the nuclear magneton for protons or the Bohr magneton for electrons. Although for electrons TE polarization can reach above 90% polarization, the significantly lower value of the proton magnetic moment makes TE much less effective for protons. For example, at a temperature of 0.5 K and a magnetic field of 5 T, the TE polarization of protons is about 1% [26].

Therefore the DNP technique is used to significantly increase nuclear polarization levels by applying microwave radiation to the target. In the UVa target, the increase in polarization is described by the equal spin temperature theory (EST). The spin temperature model is needed since the electron density is high in a solid NH_3 target and spin-spin interaction (SSI) plays an important role in the description of the system. The EST theory is summarized by Crabb and Meyer [11]. In short, within the scope of the EST theory, each energy level contains a quasi-continuous band of spin-spin states. Those bands can be characterized by a different temperature than the environment by changing the occupations of the different sub-levels using microwave radiation. The microwave radiation generates thermal mixing between the SSI temperature and nuclear Zeeman temperature, to achieve a much lower nuclear spin temperature. In practice, the target used for this experiment achieved polarization levels of between 70% and 90% under real experimental conditions.

2.1.2. Nitrogen Polarization

In a work by B. Adeva *et al.* [14] the nitrogen asymmetry in a similar ammonia target was measured relative to the proton asymmetry and compared to a calculation based on the EST model. A substantial ^{14}N polarization level of about 10% was reported for the highly polarized target, in agreement with the EST model.

3. Data Analysis

3.1. Target Polarization

An NMR system was used for continuous measurement of the proton polarization level in the target. The NMR system used in this experiment is the same as the one used in previous experiments with this target. The signal from the NMR coil was connected to a Q-meter circuit to measure the target polarization [29]. A detailed analysis of the target proton polarization is reported by D. Keller [27]. The nitrogen polarization level was calculated with respect to the proton polarization based on the EST model as calculated by Adeva et al. [14].

3.2. Optics

The standard HRS optics reconstruction procedure described in Ref. [30] is able to reconstruct the trajectories in cases where no target field is applied. In our case, a 5 T magnetic field around the target adds more complexity to the procedure. Therefore, the optics calibration and analysis is broken into two parts. The trajectories between the target and septa entrance are calculated by simulations of the electron motion in the magnetic field. The magnetic field is characterized by applying the Biot-Savart law to the current density distribution, and a cross-check is done by direct measurement of the target field. The uncertainty of the field map is less than 1.2% over the whole region [31]. The reconstruction of the trajectories from the entrance of the septa to the focal plane is done using an optics matrix. The calculation of the optics matrix is done using a sieve slit, and uses the well known behavior of elastic scattering and survey data described in [32, 33]. A simulation of the magnetic field is required for the optics matrix optimization, since linear propagation of the trajectories from the target to the sieve slit cannot be assumed.

As part of the optics analysis a GEANT4 [34] Monte-Carlo simulation of the experimental setup, g2psim, was developed [31]. The simulation contains the materials and the field map along the trajectory of the scattered electron, and was used for the calibration of the optics matrix. The trajectories are

calculated by integration of the equation of motion in the magnetic fields using the Runge-Kutta-Nyström method. Energy losses due to ionization, electron scattering, internal and external Bremsstrahlung are included in the simulation, as described in [35].

The presence of the target field results in bending of the beam upstream of the target as well. To compensate for this effect, two chicane magnets were installed to lower then lift the beam trajectory to achieve normal incidence of the electron beam on the center of the target. However, even after this correction the beam showed deviations from the center and was slightly tilted relative to the beam axis. The tilt angle was calculated using BdL simulations.

Fig. 2 shows an example of two dimensional histogram of scattered electron momentum vs. scattering angle. The elastic stripes for scattering off different nuclei (with mass M) are given by:

$$E' = \frac{E}{1 + \frac{E}{M}(1 - \cos \theta)}, \quad (4)$$

where E' is the scattered electron energy, E is the incoming beam energy, and θ is the scattering angle. An imperfect scattering angle reconstruction results in small deviation of the variables in Eq. 4 and is dealt with by applying an additional correction on the scattering angle. This correction is calculated as function of the reconstructed scattering angle by comparing to the expected scattering angle:

$$\cos \theta = 1 + M \left(\frac{1}{E} - \frac{1}{E'} \right) \quad (5)$$

around the proton elastic stripe. In this way the elastic stripe can be used for fine tuning of the optics.

This uncertainty is estimated to be ~ 1 MeV, based on the HRS resolution, electron energy loss approximation, and deviation of the invariant masses of hydrogen peaks from 0.9383 MeV. This translates into a ~ 2 mrad systematic uncertainty in the scattering angle.

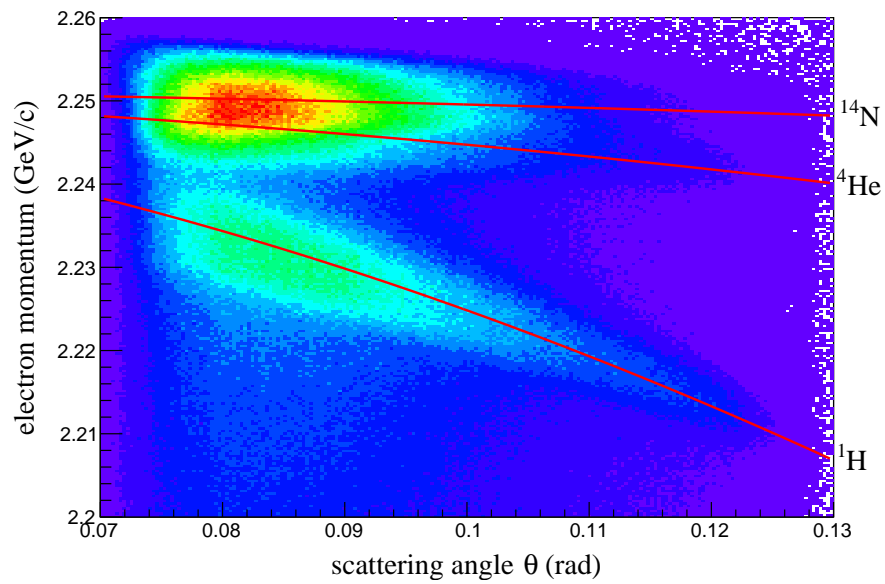


Figure 2: (colour online) Typical distribution of reconstructed momentum and scattering angle variables. The separation between elastic scattering on hydrogen and the heavier elements ^{14}N and ^4He is evident, and the red curves compare the reconstructed variables to the elastic stripe formula (Eq. 4).

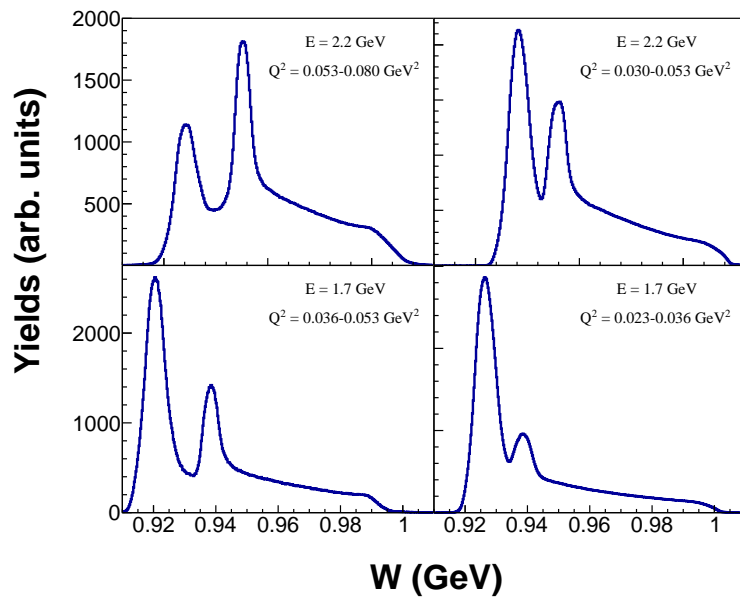


Figure 3: Invariant mass distributions for the left HRS at all experimental configurations. The hydrogen elastic events can be identified as the peak at $\sim 938 \text{ MeV}$.

3.3. Asymmetry Extraction

Fig. 3 shows the distribution of the invariant mass, W , for the different beam energy and momentum transfer values used for this analysis. The invariant mass is calculated using the target proton momentum $P^\mu = (M_p, 0, 0, 0)$ and the momentum transfer $q^\mu = k^\mu - k'^\mu$, as:

$$P_{tot}^\mu = q^\mu + P^\mu, \quad (6)$$

$$W = \sqrt{P_{\mu,tot} P_{tot}^\mu}. \quad (7)$$

The use of the invariant mass allows one-dimensional analysis that is equivalent to a two-dimensional analysis on momentum and scattering angle (Fig. 2). The invariant mass histograms are divided into three main regions: elastic scattering off ^4He and ^{14}N ($W \lesssim 0.93$ GeV), elastic scattering off ^1H ($W \sim 0.938$ GeV), and quasi-elastic scattering off ^4He and ^{14}N ($W \gtrsim 0.95$ GeV). Non-negligible mixing between the regions is due to the width of the elastic and quasi-elastic peaks, and due to radiative energy losses of the low W scattering events.

In order to calculate the relative contribution of the different scattering components, we used g2psim to simulate the invariant mass distribution of each individual component. As an input to the simulation, elastic models for protons, ^4He , and ^{14}N were coded using experiment-based form factor parameterizations [36, 37]. As inelastic scattering data at the relevant kinematics are not available, g2psim uses two models, QFS [38] and PBosted [39] as an input for the inelastic scattering simulation. The two models produced significantly different yields at the quasi-elastic region in our kinematics. Unpublished nitrogen data at similar kinematics were compared to these models, and the PBosted model was seen to better reproduce the quasi-elastic peak [40]. This was also indicated by the quasi-elastic data collected in this experiment. Consequently, for this analysis, the PBosted model was selected. Gaussian smearing on the order of 1-2 MeV (1σ) and an energy shift on the order of 0.5-1 MeV was applied to the simulated data in order to account for inaccuracies in the simulated detection resolution and energy losses. The simulation was only used to produce the shape

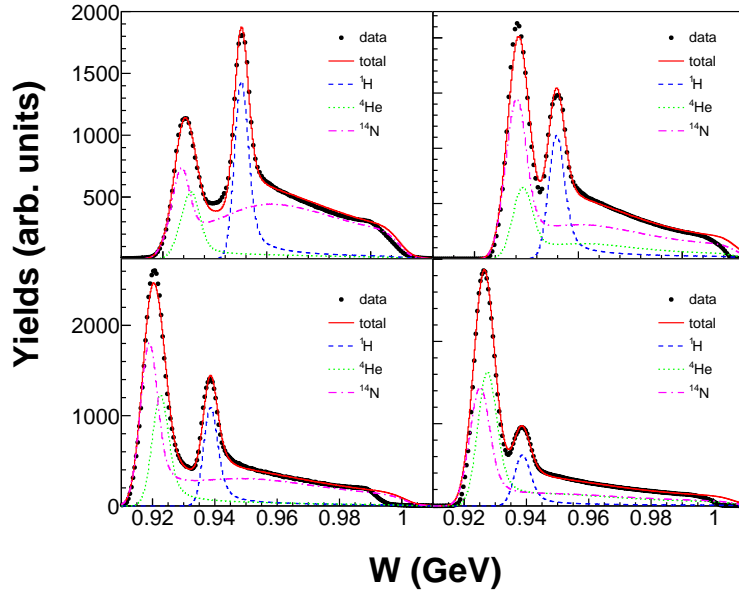


Figure 4: Simulation results for all experimental configurations. The black circles are the experimental data, the red curves are the total simulated yields, the blue, green and purple curves are the proton, helium and nitrogen partial contributions, respectively.

of the invariant mass distribution of the different scattering components. The relative amplitudes cannot be accurately derived from the cross section models, and the packing fraction (i.e., the mass ratio between helium and ammonia in the target) is only poorly known. Instead, the magnitude of each contribution is scaled to the data using a minimum χ^2 fit. Fig. 4 shows the simulation results for all experimental configurations after the correction and the fit.

The above fitting procedure is not very sensitive to the differences between ^4He and ^{14}N elastic contributions, and it is almost completely insensitive to the differences between the quasi-elastic contributions of these two elements. Nevertheless, the differentiation between the three main regions in the spectrum, heavy element elastics, proton elastics, and quasi-elastics, is robust. Hence, we

only use the combined ^4He and ^{14}N contributions for the analysis. We do not consider these fits reliable in terms of the differences between ^4He and ^{14}N yields.

For an unpolarized background B , the experimental asymmetry (assuming 100% beam and target polarization) is:

$$A_{raw} = \frac{N^+ - N^-}{N^+ + N^- + B} = \frac{A_{phys}}{1 + \frac{B}{N^+ + N^-}}, \quad (8)$$

$$A_{raw} = A_{phys} \cdot \left(1 - \frac{B}{T}\right) \quad (9)$$

where A_{raw} is the raw asymmetry, A_{phys} is the physical asymmetry, N^\pm are the number of events with positive or negative helicities, and $T = N^+ + N^- + B$ is the total event count. We define the dilution factor $f = 1 - B/T$ and add the corrections for the beam and target polarization to obtain:

$$A_{phys} = \frac{A_{raw}}{fP_B P_T}, \quad (10)$$

where P_B and P_T are beam and target polarization, respectively. In our case the polarized ^{14}N contributes to the measured asymmetry, and Eq. 10 cannot be used. B. Adeva *et al.* [14] and O. A. Rondon [15] used shell model approximations to determine the nitrogen asymmetry relative to the proton asymmetry. Here we propose a different approach, based on the measured asymmetries in the different regions of the invariant mass distribution. The data is treated as if it consists of three reactions: proton elastics, heavy-element elastics, and quasi-elastics. To each of these reactions we attribute a physical asymmetry A_1, A_2, A_3 , respectively. Each of these reactions dominates a different region in the invariant mass histogram, with some level of mixing of all three regions (see Fig. 5). Using the data we extract raw asymmetries for each region, $A_{raw,1}, A_{raw,2}, A_{raw,3}$. The raw asymmetries are related to the physical asymmetries by:

$$A_{raw,i} = \sum_{j=1}^3 C_{i,j} A_j, \quad (11)$$

where the coefficient $C_{i,j}$ is the partial contribution of reaction j to the yields in region i , and is calculated from the simulation. This set of linear equations can

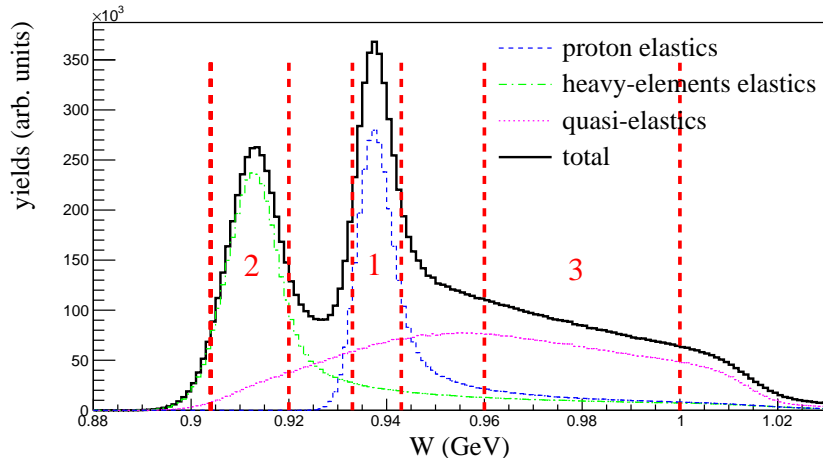


Figure 5: An example of invariant mass histogram divided into three regions, each dominated by different reaction: proton elastics (1), heavy-elements elastics (2) and quasi-elastics (3). The partial contribution of each reaction is determined based on simulation.

be solved to extract the physical asymmetries for the three reactions A_1, A_2, A_3 . The main advantage of this approach is that it is based on data, and does not require knowledge of the nitrogen polarization level and asymmetry, packing fraction, elastic or quasi-elastic absolute cross sections. It is noted, that the strengths of the three main regions are very clear in the data, and the successful reproduction of the quasi-elastic region by the simulation makes the determination of $C_{i,j}$ robust. A quantitative estimation of the uncertainties is detailed below. An additional important advantage is that we also extract, for the first time, physical asymmetries for ^{14}N elastic and quasi-elastic scattering. Indeed, the unknown level of ^4He background implies large relative uncertainties on the nitrogen asymmetries. The statistical uncertainty of the raw asymmetries is given by:

$$\Delta A = \sqrt{\frac{4N^+N^-}{(N^+ + N^-)^3}}. \quad (12)$$

The statistical uncertainties of the physical asymmetries, A_1, A_2 , and A_3 were determined using a Monte-Carlo method. For each extraction of physical asymmetries, Eq. 11 was solved 10^6 times, with $A_{raw,i}$ randomly generated around

$\times 10^{-7}$	A_1	A_2	A_3
A_1	4.66	0.21	-1.57
A_2	0.21	3.00	-0.79
A_3	-1.57	-0.79	3.07

(a) $0.053 < Q^2 < 0.080 \text{ GeV}^2$

$\times 10^{-7}$	A_1	A_2	A_3
A_1	1.92	-0.06	-0.64
A_2	-0.06	0.46	-0.16
A_3	-0.64	-0.16	1.36

(b) $0.030 < Q^2 < 0.053 \text{ GeV}^2$

$\times 10^{-7}$	A_1	A_2	A_3
A_1	6.62	0.01	-1.93
A_2	0.01	1.03	-0.48
A_3	-1.93	-0.48	4.49

(c) $0.036 < Q^2 < 0.053 \text{ GeV}^2$

$\times 10^{-7}$	A_1	A_2	A_3
A_1	0.36	-0.07	-0.86
A_2	-0.07	0.24	-0.16
A_3	-0.86	-0.16	2.13

(d) $0.023 < Q^2 < 0.036 \text{ GeV}^2$

Table 2: Covariance matrices for 2.2 GeV (top) and 1.7 GeV (bottom) configurations. See text for the meaning of A_1, A_2, A_3 . All values should be multiplied by 10^{-7} .

the experimental values with the appropriate standard deviation. The mean of the resulting distribution was used as the physical asymmetry, and the standard deviation as the statistical uncertainty. The correlations between the three reactions were also calculated by Monte-Carlo using the definition:

$$\Sigma_{i,j} = \sum_n (X_{i,n} - \bar{X}_i)(X_{j,n} - \bar{X}_j)/N, \quad (13)$$

where $X_{i,n}$ is the n^{th} calculated asymmetry for reaction i , \bar{X}_i is the mean asymmetry for reaction i , and N is the total number of events in the Monte-Carlo analysis. Table 2 shows the covariance matrices. Note the non-negligible off-diagonal elements.

The systematic uncertainties of the extraction were studied by changing the invariant mass cut width, and by changing the simulation energy and resolution calibrations in ranges that produce reasonable agreement with the data. The relative uncertainty on the nitrogen polarization is estimated to be 15%, based on the differences between the EST model and the experimental data in [14]. Nitrogen elastic and quasi-elastic asymmetries are diluted by the presence of

E (GeV)	Q^2 (GeV ²)	A (%)	ΔA_{stat} (%)	ΔA_{sys} (%)
2.2	0.053-0.080	0.66	0.54	0.32
2.2	0.030-0.053	0.62	0.21	0.30
1.7	0.036-0.053	0.76	0.29	0.36
1.7	0.023-0.036	0.49	0.14	0.24

Table 3: ¹⁴N elastic asymmetries with their absolute statistical and systematic uncertainties.

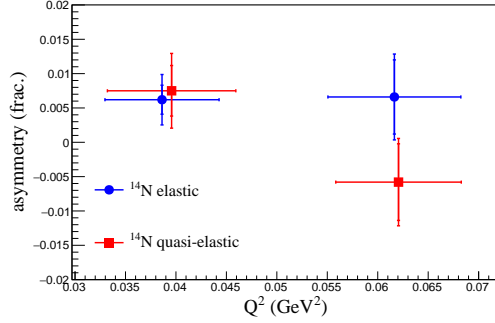
E (GeV)	Q^2 (GeV ²)	A (%)	ΔA_{stat} (%)	ΔA_{sys} (%)
2.2	0.053-0.080	-0.58	0.56	0.31
2.2	0.030-0.053	0.75	0.37	0.40
1.7	0.036-0.053	-1.82	0.61	0.97
1.7	0.023-0.036	-0.77	0.41	0.41

Table 4: ¹⁴N quasi-elastic asymmetries with their absolute statistical and systematic uncertainties.

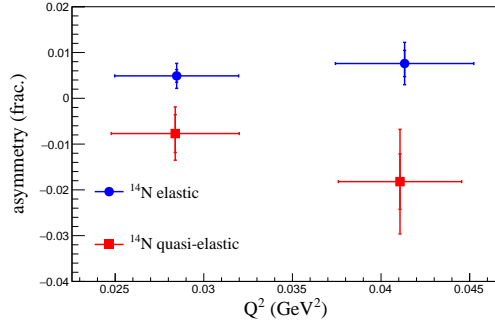
⁴He. The ratio between helium and nitrogen in the data could not be extracted from the simulation. Based on packing fraction evaluation from JLab experiment E08-027 that ran parallel to this experiment using the same target [21], and general considerations, a conservative dilution factor of $f_{14N} = 0.75 \pm 0.25$ is used in Eq. 10 to extract the physical nitrogen asymmetries.

E (GeV)	Q^2 (GeV ²)	A (%)	ΔA_{stat} (%)	ΔA_{sys} (%)
2.2	0.053-0.080	-3.57	0.061	0.142
2.2	0.030-0.053	-2.41	0.044	0.096
1.7	0.036-0.053	-2.73	0.078	0.109
1.7	0.023-0.036	-2.02	0.019	0.081

Table 5: Proton asymmetries with their absolute statistical and systematic uncertainties.



(a) $E = 2.2$ GeV



(b) $E = 1.7$ GeV

Figure 6: Physical asymmetries for electron-¹⁴N elastic (blue circles) and quasi-elastic (red squares) scattering. The horizontal error bars represents the Q^2 range of which the data was collected.

4. Results

Extracted asymmetries for electron-¹⁴N elastic scattering are listed in Table 3 and asymmetries for electron-¹⁴N quasi-elastics scattering are listed in Table 4. Fig. 6 compares both asymmetries. The extracted asymmetries for electron-proton elastics scattering are listed in Table 5. A summary of the uncertainties is given in Table 6. The magnitude of the extracted asymmetries shows general agreement with the approximations made by B. Adeva *et al.* [14] and by O. A. Rondon [15] in magnitude. However, the differences in sign between the elastic and quasi-elastic scattering requires further investigation.

origin	statistical (%)	systematic (%)
beam polarization	0.20	1.70
target polarization	0.75	2.9
asymmetry cuts	-	0-1.1
asymmetry extraction:		
nitrogen elastics	30-80	10
nitrogen quasi-elastics	30-100	25
proton elastics	0.9-5.1	2.0-3.5
^4He dilution	-	44

Table 6: A summary of asymmetry uncertainties for electron- ^{14}N elastic, electron- ^{14}N quasi-elastic, and electron-proton elastic scattering. ^4He dilution is only relevant for the nitrogen-related asymmetries. The tables list ranges over the whole data-set, and specific total uncertainties are listed in Tables 3,4,5.

5. Summary

The nitrogen in dynamically-polarized NH_3 targets contributes a nontrivial asymmetry background for high-precision measurements of lepton-proton scattering cross-section asymmetry. We experimentally extracted the nitrogen contribution for the asymmetry at Q^2 value of 0.023-0.08 GeV^2 . We also demonstrated a method for the extraction of these asymmetries that can be applied in similar experiments at different Q^2 values. The relative accuracy of our results is low, but sufficient to evaluate the absolute contribution of the nitrogen asymmetries for experiments with such targets.

Acknowledgments

This work was supported by the U.S. Department of Energy contract DE-AC05-06OR23177 under which Jefferson Science Associates operates the Thomas Jefferson National Accelerator Facility.

References

References

- [1] B. Adeva, et al., Measurement of the spin-dependent structure function $g_1(x)$ of the deuteron, Phys. Lett. B 302 (4) (1993) 533 – 539. doi:[https://doi.org/10.1016/0370-2693\(93\)90438-N](https://doi.org/10.1016/0370-2693(93)90438-N).
- [2] P. L. Anthony, et al., Determination of the neutron spin structure function, Phys. Rev. Lett. 71 (1993) 959–962. doi:[10.1103/PhysRevLett.71.959](https://doi.org/10.1103/PhysRevLett.71.959).
- [3] K. Ackerstaff, et al., Measurement of the neutron spin structure function g_{n1} with a polarized ^3He internal target, Phys. Lett. B 404 (3) (1997) 383 – 389. doi:[https://doi.org/10.1016/S0370-2693\(97\)00611-4](https://doi.org/10.1016/S0370-2693(97)00611-4).
- [4] P. Anthony, et al., Measurements of the Q^2 -dependence of the proton and neutron spin structure functions g_{1p} and g_{1n} , Phys. Lett. B 493 (1) (2000) 19 – 28. doi:[https://doi.org/10.1016/S0370-2693\(00\)01014-5](https://doi.org/10.1016/S0370-2693(00)01014-5).
- [5] S. Goertz, W. Meyer, G. Reicherz, Polarized H, D and ^3He targets for particle physics experiments, Progress in Particle and Nuclear Physics 49 (2) (2002) 403 – 489. doi:[https://doi.org/10.1016/S0146-6410\(02\)00159-X](https://doi.org/10.1016/S0146-6410(02)00159-X).
- [6] G. Warren, et al., Measurement of the electric form factor of the neutron at $Q^2 = 0.5$ and $1.0 \text{ geV}^2/c^2$, Phys. Rev. Lett. 92 (2004) 042301. doi:[10.1103/PhysRevLett.92.042301](https://doi.org/10.1103/PhysRevLett.92.042301).
- [7] V. Alexakhin, et al., The deuteron spin-dependent structure function g_{1d} and its first moment, Phys. Lett. B 647 (1) (2007) 8 – 17. doi:<https://doi.org/10.1016/j.physletb.2006.12.076>.

- [8] X. Qian, et al., Single spin asymmetries in charged pion production from semi-inclusive deep inelastic scattering on a transversely polarized ^3He target at $Q^2 = 1.4 - 2.7 \text{ GeV}^2$, Phys. Rev. Lett. 107 (2011) 072003. doi:[10.1103/PhysRevLett.107.072003](https://doi.org/10.1103/PhysRevLett.107.072003).
- [9] W. Meyer, Ammonia as a polarized solid target materials review, Nucl. Instr. Meth. A 526 (1) (2004) 12 – 21, proceedings of the ninth International Workshop on Polarized Solid Targets and Techniques. doi:<https://doi.org/10.1016/j.nima.2004.03.145>.
- [10] The Virginia/Basel/SLAC polarized target: operation and performance during experiment e143 at SLAC, Nucl. Instr. Meth. A.
- [11] D. G. Crabb, W. Meyer, Solid polarized targets for nuclear and particle physics experiments, Annu. Rev. Nucl. Part. Sci. 47 (1) (1997) 67–109. doi:[10.1146/annurev.nucl.47.1.67](https://doi.org/10.1146/annurev.nucl.47.1.67).
URL <https://doi.org/10.1146/annurev.nucl.47.1.67>
- [12] T. Averett, et al., A solid polarized target for high-luminosity experiments, Nucl. Instr. Meth. A 427 (3) (1999) 440 – 454. doi:[http://dx.doi.org/10.1016/S0168-9002\(98\)01431-4](http://dx.doi.org/10.1016/S0168-9002(98)01431-4).
- [13] G. Court, W. Heyes, The polarisation of ^{14}N and ^{15}N nuclei in polarised proton targets using irradiated ammonia, Nucl. Instr. Meth. A 243 (1) (1986) 37 – 40. doi:[https://doi.org/10.1016/0168-9002\(86\)90818-1](https://doi.org/10.1016/0168-9002(86)90818-1).
- [14] B. Adeva, et al., Measurement of proton and nitrogen polarization in ammonia and a test of equal spin temperature, Nucl. Instr. Meth. A 419 (1) (1998) 60 – 82. doi:[http://dx.doi.org/10.1016/S0168-9002\(98\)00916-4](http://dx.doi.org/10.1016/S0168-9002(98)00916-4).
- [15] O. A. Rondon, Corrections to nucleon spin structure asymmetries measured on nuclear polarized targets, Phys. Rev. C 60 (1999) 035201. doi:[10.1103/PhysRevC.60.035201](https://doi.org/10.1103/PhysRevC.60.035201).
- [16] Y. Kiselev, N. Doshita, F. Gautheron, K. Kondo, W. Meyer, Indirect detection of nitrogen spins in ammonia target at superlow temperatures, Nucl.

- Instr. Meth. A 711 (2013) 8 – 11. doi:<https://doi.org/10.1016/j.nima.2013.01.043>.
- [17] M. Friedman, *Measurement of the proton form factor ratio at low momentum transfer*, Ph.D. thesis, The Hebrew University of Jerusalem (2016).
URL <https://www.osti.gov/biblio/1408883>
- [18] T. Donnelly, A. Raskin, Considerations of polarization in inclusive electron scattering from nuclei, *Ann. Phys.* 169 (2) (1986) 247 – 351. doi:[http://dx.doi.org/10.1016/0003-4916\(86\)90173-9](http://dx.doi.org/10.1016/0003-4916(86)90173-9).
- [19] C. W. Leemann, D. R. Douglas, G. A. Krafft, *The continuous electron beam accelerator facility: CEBAF at the jefferson laboratory*, *Annu. Rev. Nucl. Part. Sci.* 51 (1) (2001) 413–450. doi:[10.1146/annurev.nucl.51.101701.132327](https://doi.org/10.1146/annurev.nucl.51.101701.132327).
URL <https://doi.org/10.1146/annurev.nucl.51.101701.132327>
- [20] J. Alcorn, et al., Basic instrumentation for hall a at Jefferson Lab, *Nucl. Instr. Meth. A* 522 (3) (2004) 294 – 346. doi:<http://dx.doi.org/10.1016/j.nima.2003.11.415>.
- [21] M. A. Cummings, *Investigating proton spin structure: A measurement of g_2^p at low Q^2* , Ph.D. thesis, The College of William and Mary (2016).
URL <https://scholarworks.wm.edu/etd/1477067907/>
- [22] M. Baylac, et al., First electron beam polarization measurements with a compton polarimeter at Jefferson Laboratory, *Phys. Lett. B* 539 (12) (2002) 8 – 12. doi:[http://dx.doi.org/10.1016/S0370-2693\(02\)02091-9](http://dx.doi.org/10.1016/S0370-2693(02)02091-9).
- [23] Møller measurements for E08-027 (g2p) and E08-007, Tech. rep. (2012).
- [24] O. A. Rondón, The RSS and SANE experiments at Jefferson Lab, in: *AIP Conference Proceedings*, Vol. 1155, 2009.
- [25] A. W. Overhauser, Polarization of nuclei in metals, *Phys. Rev.* 92 (1953) 411–415. doi:[10.1103/PhysRev.92.411](https://doi.org/10.1103/PhysRev.92.411).

- [26] V. A. Atsarkin, Dynamic nuclear polarization: Yesterday, today, and tomorrow, *J. Phys.: Conf. Ser.* 324 (2011) 012003. doi:[10.1088/1742-6596/324/1/012003](https://doi.org/10.1088/1742-6596/324/1/012003).
- [27] D. Keller, Uncertainty minimization in nmr measurements of dynamic nuclear polarization of a proton target for nuclear physics experiments, *Nucl. Instr. Meth. A* 728 (2013) 133 – 144. doi:<https://doi.org/10.1016/j.nima.2013.06.103>.
- [28] J. Pierce, J. Maxwell, C. Keith, Dynamically polarized target for the g2pand gepexperiments at jefferson lab, *Phys. Part. Nuclei* 45 (1) (2014) 303–304. doi:[10.1134/S1063779614010808](https://doi.org/10.1134/S1063779614010808).
- [29] G. Court, D. Gifford, P. Harrison, W. Heyes, M. Houlden, A high precision Q-meter for the measurement of proton polarization in polarised targets, *Nucl. Instr. Meth. A* 324 (3) (1993) 433 – 440. doi:[http://dx.doi.org/10.1016/0168-9002\(93\)91047-Q](http://dx.doi.org/10.1016/0168-9002(93)91047-Q).
- [30] N. Liyanage, [Calibration of the Hall A High Resolution Spectrometers using the new optimizer](#), Tech. rep., Jefferson Lab, Newport News, VA, United States (July 2002).
URL <http://hallaweb.jlab.org/publications/Technotes/files/2002/02-012.pdf>
- [31] C. Gu, [The spin structure of the proton at low \$Q^2\$: A measurement of the structure function \$g_2^p\$](#) , Ph.D. thesis, University of Virginia (2016).
URL https://libraetd.lib.virginia.edu/public_view/6h440s441
- [32] [Survey report a1453](#), Tech. rep.
URL <http://hallaweb.jlab.org/experiment/g2p/survey/>
- [33] [Survey report a1465](#), Tech. rep.
URL <http://hallaweb.jlab.org/experiment/g2p/survey/>

- [34] S. Agostinelli, et al., Geant4a simulation toolkit, Nucl. Instr. Meth. A 506 (3) (2003) 250 – 303. doi:[https://doi.org/10.1016/S0168-9002\(03\)01368-8](https://doi.org/10.1016/S0168-9002(03)01368-8).
- [35] J. Liu, [Radiation effects in simulation](#), Tech. rep., University of Virginia (May 2015).
URL http://hallaweb.jlab.org/experiment/g2p/collaborators/jie/2015_05_13_simu_rad_technotes/radiation_simulation_technotes.pdf
- [36] J. Arrington, Implications of the discrepancy between proton form factor measurements, Phys. Rev. C 69 (2004) 022201. doi:[10.1103/PhysRevC.69.022201](https://doi.org/10.1103/PhysRevC.69.022201).
- [37] C. D. Jager, H. D. Vries, C. D. Vries, Nuclear charge and moment distributions nuclear charge- and magnetization-density-distribution parameters from elastic electron scattering, At. Data Nucl. Data Tab. 14 (5) (1974) 479 – 508. doi:[http://dx.doi.org/10.1016/S0092-640X\(74\)80002-1](http://dx.doi.org/10.1016/S0092-640X(74)80002-1).
- [38] J. W. Lightbody, J. S. OConnell, Modeling single arm electron scattering and nucleon production from nuclei by GeV electrons, Computers in Phys. 2 (3) (1988) 57–64. doi:<http://dx.doi.org/10.1063/1.168298>.
- [39] P. E. Bosted, V. Mamyan, Empirical Fit to electron-nucleus scattering, ArXiv e-prints [arXiv:1203.2262](https://arxiv.org/abs/1203.2262).
- [40] R. Zielinski, [The \$g_2^p\$ experiment: A measurement of the protons spin structure functions](#), Ph.D. thesis, The University of New Hampshire (2016).
URL <https://arxiv.org/pdf/1708.08297.pdf>